A DFT studies on a potential anode compound for Li-ion batteries*: Hexa-cata-*

hexabenzocoronene nanographene

Behlol Hashemzadeh [a], Ladan Edjlali [a], Parvaneh Delir Kheirollahi-Nezhad [b], Esmail Vessally [b, *]

[a] Department of Chemistry, Tabriz Branch, Islamic Azad University, Tabriz, Iran
[b] Department of Chemistry, Payame Noor University, Tehran, Iran

ARTICLE INFO

ABSTRACT

In this work, the possible apply of a hexa-cata-hexabenzocoronene HCor as anode material was studied for Li-ion batteries (LIBs) using the B3LYP/6-31G* level. The planar structure of HCor is less stable (by about 0.243 hartree) in comparison with the twisted structure. The Li cation and neutral are suitably adsorbed high up the middle of a HCor hexagonal ring with the adsorption energy of -120.3 and -2.7 kcal/mol, respectively. The calculated specific storage capacity of HCor is 450.1 mAh/g and the great cell voltage is 2.63 V generated by the interaction between Li+ and HCor. The HCOR is considered an ideal candidate to be used as an anode material in LIBs because of high storage capacity and ion mobility.

1. Introduction

Currently, the need for sustainable and cost-effective energy storage materials drives battery research. Rechargeable Li-ion batteries (LIBs) are the most well-known batteries, and they have witnessed great advances in technology. They have drawn vast interest because of their applicability in portable energy storage devices, electronics, electrical and hybrid electrical vehicles, etc. [1]. Although LIBs have some excellent features, they also impose some limitations since they are expensive to manufacture, subject to aging and safety issues [2-11]. Na-, K-, and Mg-ion batteries can be considered as ideal alternatives to LIBs [12-15]. These metals are more abundant and cheaper than Li, and have better safety features. Magnesium is more attractive because of transporting twice as much charge per atom. However, manufacturing MIBs faces difficulties since proper electrode materials are hard to find.

Nanomaterials, which display unique features, accelerate the development of electronic devices, power supplies, and optic systems [16-25].

Nanostructures, in the form of nanofilms, graphene, nanobelts, nanoflakes, nanoparticles, nanorings, etc., have been investigated in order to be used in ion batteries [25-34]. Recently, nanographene has been investigated as a substitute for graphene [35]. Unlike graphene, nanographene has a finite or limited structure without dimension. Also, nanographene has been considered as a promising candidate to be used in various fields including diodes, photovoltaics, transistors, and electronics, owing to its film-forming properties, ultra-high surface area, elevated charge carrier mobility, and unique chemical properties [35].

It has been previously shown that nanographenes such as hexa-peri-hexabenzocoronene (HBC) nanographene functionalized with –NH_2 group is an appropriate anode material for application in the LIBs [36]. In 2019, the synthesis of hexa-cata-hexabenzocoronene nanographene (HCOR) and its poly-substituted structures from tetraryl olefins was carried out through iron chloride-and iodine-catalyzed oxidative cyclodehydrogenation reactions [37].

The HCOR shows a p-type field-effect mobility that ranged from 0.34 to 0.51 cm^2/Vs, and the on/off current ratio was 105−107, indicating its potential applications as conducting channels for a transistor [37]. In the current study, possibility of using HCOR as anode material for MIBs was investigated by implementing density functional theory (DFT).

2. Computational methods

∗ Corresponding author. e-mail: vessallyesmail@gmail.com

B3LYP-gCP-D3/6-31G* method was implemented to carry out the calculations in terms of energy, electricity, charge transfer, and structure optimizations. The standard B3LYP functional has a major drawback which has been implemented for different aims, i.e. dispersion interaction assessment [38]. However, the B3LYP-gCP-D3 scheme removes a major deficiency, i.e. basis set superposition error [39]. The gCP which represents *geometrical counterpoise correction* provides an estimate of both inter- and *intra*molecular BSSE. For a given HCOR or its complex with Li or Li^{1+}, The B3LYP-gCP-D3 energy is computed according to the following equation:

$$E^{B3LYP-gCP-D3} = E^{B3LYP} + E^{gCP} + E^{D3}$$
$$(1)$$

To calculate the adsorption energy (AE) of Li/Li^{1+}@HCOR configurations, the following equation was used:

$$E_{ad} = E(Li/Li^{1+}@HCOR) – E(HCOR) – E(Li/Li^{1+})$$
$$(2)$$

For detailed methodology see reference [39]. *Synchronous Transit-Guided Quasi-Newton* (STQN) method was used in order to measure the energy of the transition states (TS) [40]. The GAMESS program is applied to carry out all of the computations [41]. The GaussSum software application was employed to plot the density of states (DOS) [42].

3. Results and discussion

3.1. Li cation adsorption on the HCOR

The HCOR (Fig. 1) has 48 C and 24 H atoms with a non-planar structure (unlike the HCOR which is planar) in which six rim benzene rings alternately bent up and down with respect to the central coronene part. The planar structure of HCOR is unstable by about 152.5 kcal/mol based on our calculations owing to the steric effect of hydrogen atoms. Three hexagonal rings are recognized in the HCOR structure, labeled **a**, **b**, and **c** as shown in Fig. 1. According to Fig. 1, it can be seeming that the Eg of HCOR is 3.33 eV with THE LUMO and HOMO energies -5.10 and -1.77 eV, respectively (Table 1). The calculated Eg for HCOR is substantial in contrast with the graphene,

so HCOR is suitable for various applications in different fields. The Li cation was initially situated at different places on the HCOR surface to get the most stable structures in Li^{1+}@HCOR complexes. These placed include atop the carbon atoms, on the C-C bond bridge sites and, atop the center of **a**, **b**, and **c** hexagons. In Fig. 2, ultimate optimized complexes for Li^{1+}@HCOR complexes are displayed, showing the preferential deposition of Li cation atop **a**, **b**, and **c** hexagons, designated by **I**, **Π**, and **Ⅲ** complexes, respectively. In complex **I**, the Li cation is adsorbed onto hexagon **a** and the AE is -200.3 kcal/mol. The Li^{+1} is placed at the center of ring **a** and the interaction distance is 2.11 Å. The minimum distance between the HCOR surface and the Li atom or cation is characterized as the interaction distance.

The bonds of the adsorbing rings are lengthened after the adsorption of Li^{1+} by about 0.01-0.03 Å because charge transfer of about 1.121 e (complex **I**) occurs from the π-electrons of HCOR to the Li cation through a cation-π interaction. Also, the subtraction of the single point energy of bare HCOR from the single point energy of HCOR yielded the deformation energy which showed the influence of the adsorption process on the HCOR geometry following the elimination of Li/Li^{1+} from its complex forms. For complex **I**, the deformation energy was predicted to be 18.9 kcal/mol, which shows that the structural distortion is minor. In complex **Π**, the Li cation is adsorbed above ring **b** with AE of -199.6 kcal/mol (Table 1) and the interaction distance of about 2.12 Å (Fig. 2), demonstrating the higher stability of complex **I**. The strong interaction of Li cation with the ring **a** is due to the more flexibility and accessibility of these rings. Also, the charge transfer from the hydrogen atoms to the rings **a** increases the electron density on their surface which makes them more favorable for Li cation adsorption. In the complex **Ⅲ**, the Li cation is adsorbed above a hexagonal ring **c** with the interaction distance of about 2.15 Å (Fig. 2) and the AE of -198.5 kcal/mol. The BSSE has a negligible impact on the Li cation AEs, *i.e.* 1.0-1.2 kcal/mol, but dispersion term (D3) affects the Li cation AEs in a sensible way (~ -6.2 to -6.7 kcal/mol).
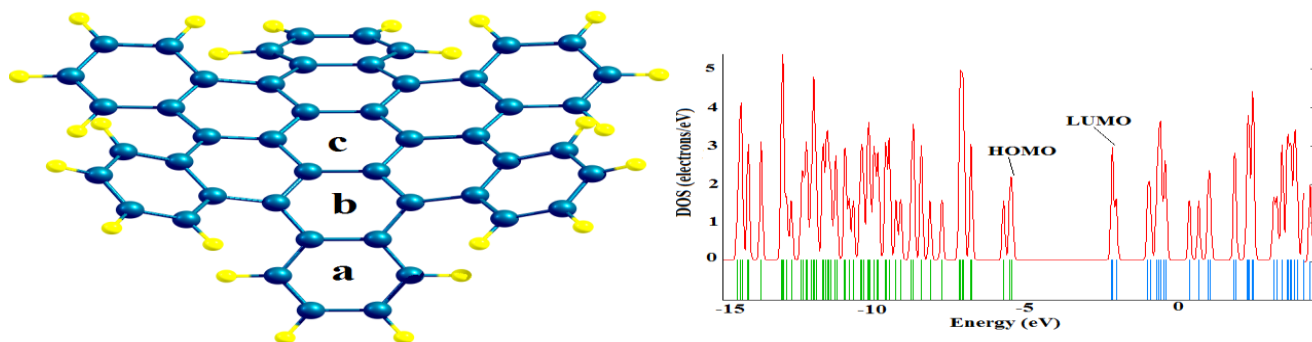
Fig. 1. Optimized structures of HCOR and its density of states plot.

3.2. Energy barriers

The ion mobility on the electrode surface is a significant property which should be taken into account to assess the appropriateness of an anode material to be used in an ion battery. The mobility as well as the diffusion of the ion on the electrode affect the rate of charge and discharge. Main paths for Li cation migration on the surface of HCOR are displayed in Fig. 3, and the energy barriers are calculated. The energy barrier corresponding to 6.2 kcal/mol must be overcome by the Li cation to transfer from the surface of ring **a** to that of **b** (path 1), which crosses over a bond C-C. The Li cation adsorption onto ring **a** surface is more stable compared to ring **b** by about 0.7 kcal/mol. Hence, the Li cation will overcome the energy barrier of about 6.9 kcal/mol to migrate in a reverse path (**b** to **a**).

Table 1. The adsorption energies, of Li/Li^{1+} (E_{ad}, kcal/mol) on the HCOR. Deformation energies (E_{def}), basis set superposition errors (BSSE), and dispersion corrections (D3) are in kcal/mol. Energies of HOMO, LUMO and HOMO-LUMO gap (E_g) in eV. ΔE_g indicates the change of E_g of HCOR after the Li/Li^{1+} adsorption. Q indicates the NBO charge on the Li species in the complex form.

Adsorbate	Structure	E_{ad}	E_{def}	BEES	D3	E_{HOMO}	E_{LUMO}	E_g	%ΔE_g	Q(e)
-	HCOR	-	-	-	-	-5.10	-1.77	3.33	-	-
Li^{1+}	**I**	-200.3	18.9	1.0	-6.5	-10.18	-9.59	0.59	-82.3	0.879
	II	-199.6	18.0	1.2	-6.7	-10.15	-9.48	0.67	-79.9	0.891
	III	-198.5	17.2	1.2	-6.2	-1.05	-9.42	0.63	-81.1	0.895
Li	i	-4.5	1.2	0.3	-3.2	-4.96	-1.79	3.17	-4.8	0.020
	ii	-4.7	1.1	0.2	-3.3	-4.89	-1.78	3.11	-6.6	0.015
	iii	-4.0	1.0	0.3	-3.2	-4.87	-1.78	3.09	-7.2	0.022
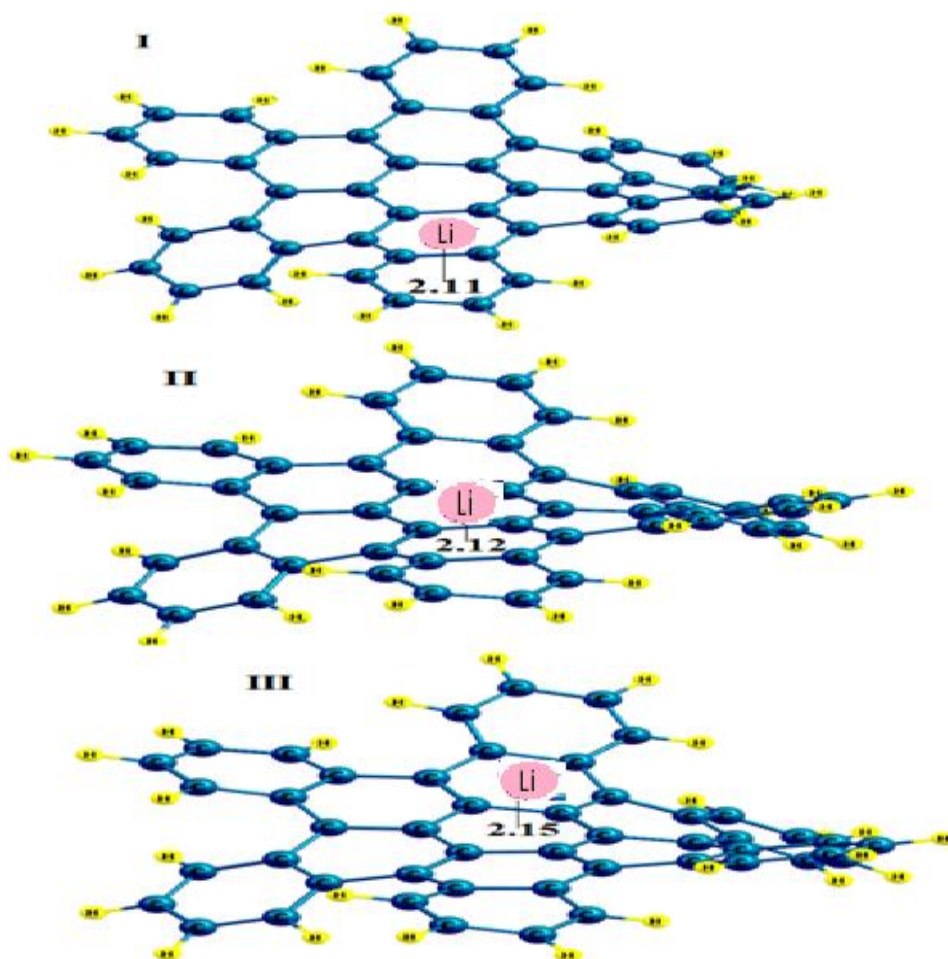
Fig. 2. Optimized structures of Li @HCOR complexes. Distances are in Å.
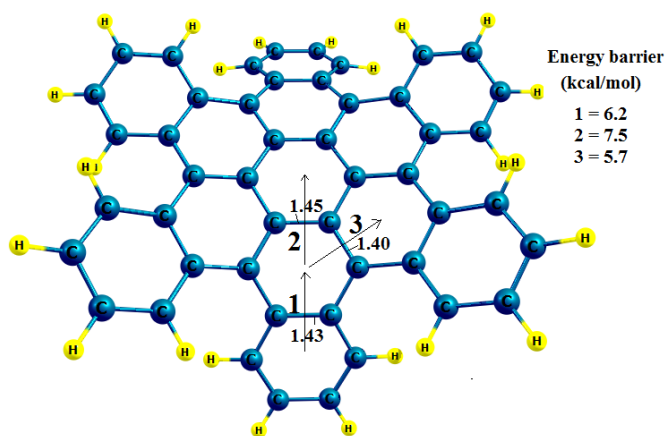
Fig. 3. Schematic view of transferring an Li cation on the surface of HCOR via different paths.

The predicted energy barrier for migration of Li cation (path 2) from the ring **b** to the ring **c** is 7.5 kcal/mol, and that is about 5.7 kcal/mol for path 3. It can be seen that there exists a reverse relation between the energy barrier and the lengths for C-C bonds which Li cation has to cross over them. The calculated C-C bond lengths are 1.43, 1.45, and 1.40 Å for paths 1, 2, and 3, respectively. The stronger cation-π interaction in the shorter C-C bonds more stabilizes the Li^{1+}/HCOR transition state structures, reducing the energy barrier. In general, an increase is observed in the ion mobility and charge/discharge rate due to the unsubstantial energy barriers. Li cation diffusion coefficient (D) was investigated on the HCOR for the sake of further instigation using the equation below [43, 44]:

$$D = l^2 v_0 \exp\left(-E_{act}/k_B T\right)$$

(3)

where E_{act} represents the diffusion barrier, l represents the migration distance, and the vibrational frequency is represented by v_0 which is normally set to 10^{13} Hz. k_B represents the Boltzmann's constant and T represents the temperature. The migration distances via path 1, 2, and 3 are approximately 2.42, 2.43, and 2.45 Å, respectively. Thus, the expected diffusion coefficients are about 1.69×10^{-7}, 1.90×10^{-8}, and 4.02×10^{-7} cm²/s, respectively, which shows that the HCOR yields a high ion mobility and this causes a fast rate of charge and discharge.

3.3. The adsorption of Li atom

To study the adsorption of Li atom onto the HCOR, different adsorption places are taken into account as Li cation adsorption. Similar to the Li^{1+} adsorption, three stable configurations were found for Li@HCOR, labeled as ⅰ, ⅱ, and ⅲ matching to the **I**, **II**, and **III** complexes, respectively. In these configurations, the Li atom is localized atop the middle of **a**, **b**, and **c** rings at a distance of 4.17, 4.18 and 4.20 Å, respectively, with AEs about -4.5, -4.7, and -4.0 kcal/mol (Table 1). The BSSE affects the Li AEs to a negligible extent, *i.e.* 0.4 kcal/mol, but the impact of the dispersion term (D3) is substantial (~ -3.3 kcal/mol). This shows that the main

interaction between the HCOR and the Li atom is non-. As a comparison, the AE of Li atom onto the graphene was about -3.9 kcal/mol, which was computed by using M06-2X/6-31G* method [45]. Deformation energy is less than 1.3 kcal/mol (Table 1) for all of the Li adsorption processes, which is negligible. The interaction of Li cation with the HCOR (in comparison with atomic Li) is stronger due to the fact that the HCOR has an electron-rich surface on which the delocalized π-electrons have a powerful tendency to target species that are electron-deficient like cations. However, Li atom has the tendency to donate its valence electron to an electron-poor surface. A small charge transfer to the HCOR from the Li atom after a physisorption process, which is about 0.01-0.03 *e*.

To investigate the biggest Li storage capacity for HCOR, various Li atom adsorptions onto the HCOR are scrutinized. The findings show that in the stable complex, for the biggest Li storage, six Li atoms are adsorbed onto six **a** rings at the same time, and three Li atoms are alternatively adsorbed onto three **b** rings. However, according to in Fig. 4, Li atoms are adsorbed onto the opposite surface of HCOR in the latter case. The calculated average AE per Li atom is about -3.5 kcal/mol for the final complex $Li_9C_{48}H_{24}$. The calculated mean Li…Li distance in the obtained complex is in the range of 4.66-4.83 Å which is much larger than that in the dimagnesium (Li_2, ~ 3.92 Å). The specific storage capacity (C) is computed as follows:

$$C = nxF/M_f$$

(4)

where M_f represents the mass of formula of unit $LiC_{5.33}H_{2.67}$, x represents the number of Li atoms, n represents the number of transferred electrons, and F represents the Faraday constant. Therefore, the specific capacity of HCOR is 589.4 mAh/g. As a comparison, we collected the storage capacity of some anode materials for MIBs, including Hollandite–MnO_2 (475 mAh/g) [46], Bi (350 mAh/g) [47], bilayer arsenene (537 mAh/g) [48],

C₃N graphene-like sheet (~ 319 mAh/g) [49], and Li₄Ti₅O₁₂ (175 mAh/g) [50].
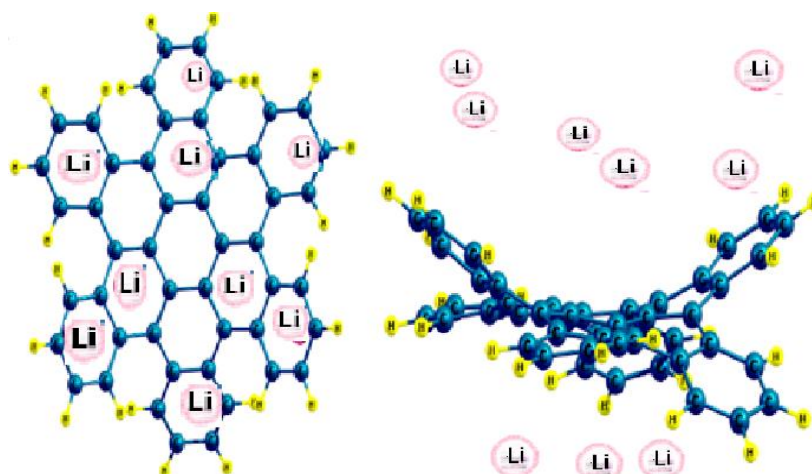
Fig. 4. Side and top views of optimized structure of 9Li@HCOR complexes.

3.4. Electronic properties

The electronic HCOR properties are dramatically interrupted via Li as well as Li^{1+}, but in a different way (Table 1). For example, after the Li adsorption onto the HCOR via complex **i**, its HOMO shifts from −5.37 to -4.96 eV in a noticeable way, but the LUMO does not change. Partial DOS plot for complex **i** shows that a new electronic peak is generated at -4.96 eV, which chiefly comes from the contribution of Li atom. Also, the frontier molecular orbital shapes in Fig. 5 approve that the HOMO localizes on the Li atom, but the LUMO is

still located on the HCOR in complex **i**. Unlike the Li atom, the HOMO and LUMO of HCOR were shifted to lesser energies by Li^{1+} adsorption, and reducing its E_g. To give an instance, in complex **I**, in the bare HCOR, the HOMO level is changed from -5.10 to -10.18 eV and the LUMO levels is changed from -1.77 eV to -9.56 eV (Table 1). By the Li^{1+} adsorption, the E_g of HCOR is decreased from 3.33 to 0.59 eV in complex **I** since its storage capacity and ion mobility is high, and it has a large cell voltage.
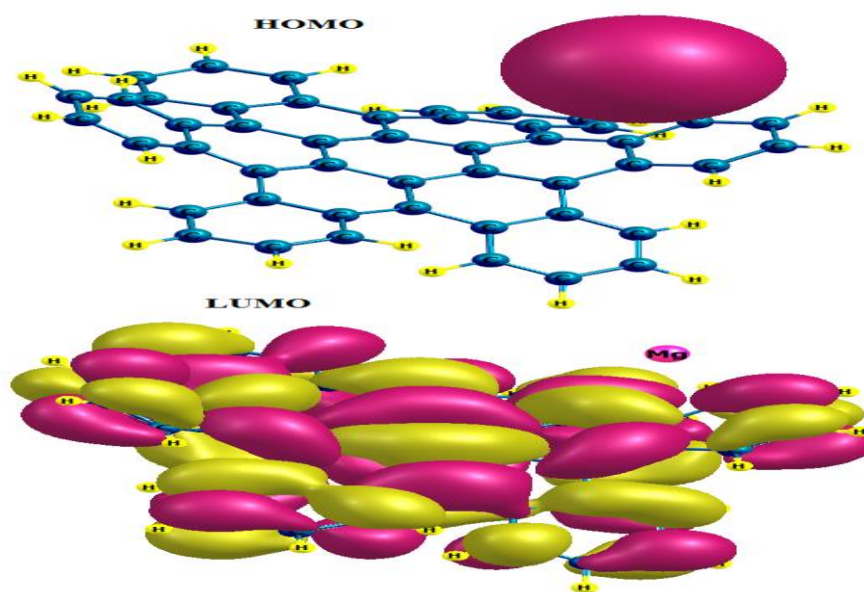
Fig. 5. HOMO and LUMO profiles of Li@HCOR complex (**i**).

3.5. Cell voltage

Higher energy density as well as particular capacity for energy storage require a high cell voltage. These parameters are of paramount importance to improve the

performance of an ion-battery. In case HCOR is implemented as the MIB anode electrode, the reactions in the cathode and anode can be termed as follows: (in the anode) Li@HCOR ↔ Li^{1+}@HCOR + 2e⁻, and (in the

cathode) $Li^{1+} + 2e^- \leftrightarrow Li$. Now, the overall reaction is expressed as:

$$Li^{1+} + Li@HCOR \leftrightarrow Li^{1+}@HCOR + Li + \Delta G_{cell} \quad (5)$$
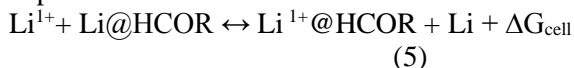
Nernst expression is incorporated to compute the cell voltage:

$$V_{cell} = - \Delta G_{cell}/zF \quad (6)$$

$$\Delta G_{cell} = \Delta E_{cell} + P\Delta V_{cell} - T\Delta S_{cell} \quad (7)$$

The volume and entropy contributions on the cell voltage were calculate to be less than 0.01 V, which is insignificant [51]. Thus, by excluding $P\Delta V_{cell}$ and $T\Delta S_{cell}$, we will have:

$$\Delta E_{cell} \sim \Delta G_{cell} = E(Li) + E(Li^{1+}@HCOR) - E(Li^{1+}) - E(Li@HCOR) \quad (8)$$

According to Eq. 8, a larger cell voltage will be produced in case the interaction of Li^{+1} with the HCOR becomes strong. But, as mentioned above, the Li^{1+} adsorption onto the HCOR is much stronger in comparison with the Li atom. The calculated ΔE_{cell} is -195.6 kcal/mol and cell voltage is 4.23 V for MIBs. The stronger cation-π interaction between Li^{1+} and the HCOR yields a high cell voltage for MIBs. Thus, the HCOR can be considered as a future prospect to be implemented as anode material for MIBs since it has high ion mobility, large cell voltage, as well as excellent storage capacity.

4. Conclusions

The possibility of HCOR application was investigated as anode for MIBs implementing the B3LYP-gCP-D3 method. The AEs of Li or Li^{1+} on the HCOR were computed to be -4.7 or -200.3 kcal/mol, on a hexagonal ring. The dispersion term is much more significant for the adsorption of atomic magnesium in comparison to its cation. The Li^{1+} migration maximum energy barrier on the surface of HCOR was found to be 7.5 kcal/mol with the ion diffusion coefficient of about 1.90×10^{-8} cm^2/s. The calculated cell voltage is are 4.23 V and the specific storage capacity is 589.4 mAh/g for the HCOR. The cell voltage in MIBs is high, owing to the fact that the cation–π interaction between the π-electron-rich HCOR and Li^{1+} the is strong. Our results demonstrate that the HCOR can be implemented as an ideal anode substance in MIBs since its cell voltage and storage capacity is high, and it has good ion mobility.

References

[1] J.R. Dahn, T. Zheng, Y. Liu, J. Xue, Mechanisms for lithium insertion in carbonaceous materials, Science, 270 (1995) 590.

[2] M.D. Johannes, K. Swider-Lyons, C.T. Love, Oxygen character in the density of states as an indicator of the stability of Li-ion battery cathode materials, Solid State Ionics, 286 (2016) 83-89.

[3] M. Armand, J.-M. Tarascon, Building better batteries, Nature, 451 (2008) 652-657.

[4] H. Kim, J.C. Kim, M. Bianchini, D.H. Seo, J. Rodriguez-Garcia, G. Ceder, Recent progress and perspective in electrode materials for K- ion batteries, Advanced Energy Materials, 8 (2018) 1702384.

[5] P.P. Prosini, C. Cento, M. Carewska, A. Masci, Electrochemical performance of Li-ion batteries assembled with water-processable electrodes, Solid State Ionics, 274 (2015) 34-39.

[6] Q. Deng, Y. Wang, Y. Zhao, J. Li, Disodium terephthalate/multiwall-carbon nanotube nanocomposite as advanced anode material for Li-ion batteries, Ionics, 23 (2017) 2613-2619.

[7] N.P. Shetti, S. Dias, K.R. Reddy, Nanostructured organic and inorganic materials for Li-ion batteries: A review, Materials Science in Semiconductor Processing, 104 (2019) 104684.

[8] T. Huang, B. Tian, J. Guo, H. Shu, Y. Wang, J. Dai, Semiconducting borophene as a promising anode material for Li-ion and Na-ion batteries, Materials Science in Semiconductor Processing, 89 (2019) 250-255.

[9] Levi, E.; Gofer, Y.; Aurbach, D. On the Way to Rechargeable Mg Batteries: The Challenge of New Cathode Materials. Chem. Mater. 2009, 22, 860–868.

[10] Barker, J.; Saidi, M. Y.; Swoyer, J. L. A Sodium-Ion Cell Based on the Fluorophosphate Compound NaVPO4F. Electrochem. Solid-State Lett. 2003, 6, A1–A4.

[11] D. Er, J. Li, M. Naguib, Y. Gogotsi, V.B. Shenoy, Ti$_3$C$_2$ MXene as a high capacity electrode material for metal (Li, Na, K, Ca) ion batteries, ACS applied materials & interfaces, 6 (2014) 11173-11179.

[12] N. Singh, T.S. Arthur, C. Ling, M. Matsui, F. Mizuno, A high energy-density tin anode for rechargeable magnesium-ion batteries, Chemical communications, 49 (2013) 149-151.

[13] M.M. Huie, D.C. Bock, E.S. Takeuchi, A.C. Marschilok, K.J. Takeuchi, Cathode materials for magnesium and magnesium-ion based batteries, Coordination Chemistry Reviews, 287 (2015) 15-27.

[14] R.C. Massé, E. Uchaker, G. Cao, Beyond Li-ion: electrode materials for sodium-and magnesium-ion batteries, Science China Materials, 58 (2015) 715-766.

[15] J.O. Besenhard, M. Winter, Advances in battery technology: Rechargeable magnesium batteries and novel negative-electrode materials for lithium ion batteries, ChemPhysChem, 3 (2002) 155-159.

[16] M.T. Baei, A.A. Peyghan, Z. Bagheri, A computational study of AlN nanotube as an oxygen detector, Chin. Chem. Lett., 23 (2012) 965–968.

[17] V. Nagarajan, R. Chandiramouli, Detection of trace level of hazardous phosgene gas on antimonene nanotube based on first-principles method, Journal of Molecular Graphics and Modelling, 88 (2019) 32-40.

[18] P.N. Samanta, K.K. Das, QM/MM study of the interaction between zigzag SnC nanotube and small toxic gas molecules, International Journal of Quantum Chemistry, 116 (2016) 411-420.

[19] O.V. Ogloblya, Y.I. Prylutskyy, Y.M. Strzhemechny, Peculiarities of conductance of carbon nanotube-based quantum dots, International Journal of Quantum Chemistry, 110 (2010) 195-201.

[20] Y.-X. Yu, Can all nitrogen-doped defects improve the performance of graphene anode materials for lithium-ion

batteries?, Physical Chemistry Chemical Physics, 15 (2013) 16819-16827.

[21] R.A. Jishi, C.T. White, J.W. Mintmire, Endohedral selenium chains in carbon, boron nitride, and BC2N nanotubes, International Journal of Quantum Chemistry, 80 (2000) 480-485.

[22] K. Adhikari, A.K. Ray, On the existence and stability of double-walled armchair silicon carbide nanotubes, Solid State Communications, 151 (2011) 430-435.

[23] A.A. Peyghan, J. Beheshtian, The influence of Stone-Wales defects in nanographene on the performance of Na-ion batteries, Journal of Molecular Graphics and Modelling, 98 (2020) 107578.

[24] A.A. Peyghan, H. Soleymanabadi, M. Moradi, Structural and electronic properties of pyrrolidine-functionalized [60]fullerenes, Journal of Physics and Chemistry of Solids, 74 (2013) 1594-1598.

[25] V.R. Cervellera, M. Albertí, F. Huarte-larrañaga, A molecular dynamics simulation of air adsorption in single-walled carbon nanotube bundles, International Journal of Quantum Chemistry, 108 (2008) 1714-1720.

[26] J. Beheshtian, M. Noei, H. Soleymanabadi, A.A. Peyghan, Ammonia monitoring by carbon nitride nanotubes: A density functional study, Thin Solid Films, 534 (2013) 650–654.

[27] B. Shang, Q. Peng, X. Jiao, G. Xi, X. Hu, TiNb2O7/carbon nanotube composites as long cycle life anode for sodium-ion batteries, Ionics, 25 (2019) 1679-1688.

[28] F. Akbari, M. Foroutan, The effect of two layers of graphene with a striped pattern on wettability parameters of the biodroplets, Adsorption, 26 (2020) 407-427.

[29] S. Aslam, R.U.R. Sagar, Y. Liu, T. Anwar, L. Zhang, M. Zhang, N. Mahmood, Y. Qiu, Graphene decorated polymeric flexible materials for lightweight high areal energy lithium-ion batteries, Applied Materials Today, 17 (2019) 123-129.

[30] Ş. Karaal, H. Köse, A.O. Aydin, H. Akbulut, The effect of LiBF4 concentration on the discharge and stability of LiMn2O4 half cell Li ion batteries, Materials Science in Semiconductor Processing, 38 (2015) 397-403.

[31] A.A. Peyghan, M. Noei, A Theoretical Study of Lithium-intercalated Pristine and Doped Carbon Nanocones, Journal of the Mexican Chemical Society, 58 (2014) 46-51.

[32] Z. Yang, Y. Huang, J. Hu, L. Xiong, H. Luo, Y. Wan, Nanocubic CoFe2O4/graphene composite for superior lithium-ion battery anodes, Synthetic Metals, 242 (2018) 92-98.

[33] S.W. Lee, N. Yabuuchi, B.M. Gallant, S. Chen, B.-S. Kim, P.T. Hammond, Y. Shao-Horn, High-power lithium batteries from functionalized carbon-nanotube electrodes, Nat. Nanotech. 5 (2010) 531-537.

[34] L. Yan, J. Yu, H. Luo, Ultrafine TiO2 nanoparticles on reduced graphene oxide as anode materials for lithium ion batteries, Applied Materials Today, 8 (2017) 31-34.

[35] A. Narita, X.-Y. Wang, X. Feng, K. Müllen, New advances in nanographene chemistry, Chemical Society Reviews, 44 (2015) 6616-6643.

[36] X. Wu, Z. Zhang, H. Soleymanabadi, Substituent effect on the cell voltage of nanographene based Li-ion batteries: A DFT study, Solid State Communications, 306 (2020) 113770.

[37] S. Kumar, S. Pola, C.-W. Huang, M.M. Islam, S. Venkateswarlu, Y.-T. Tao, Polysubstituted Hexa-cata-hexabenzocoronenes: Syntheses, Characterization, and Their Potential as Semiconducting Materials in Transistor Applications, The Journal of Organic Chemistry, 84 (2019) 8562-8570.

[38] J.S. Wright, C. Rowley, L. Chepelev, A 'universal'B3LYP-based method for gas-phase molecular properties: bond dissociation enthalpy, ionization potential, electron and proton affinity and gas-phase acidity, Molecular Physics, 103 (2005) 815-823.

[39] H. Kruse, L. Goerigk, S. Grimme, Why the standard B3LYP/6-31G* model chemistry should not be used in DFT calculations of molecular thermochemistry: understanding and correcting the problem, The Journal of organic chemistry, 77 (2012) 10824-10834.

[40] C. Peng, H. Bernhard Schlegel, Combining Synchronous Transit and Quasi-Newton Methods to Find Transition States, Israel Journal of Chemistry, 33 (1993) 449-454.

[41] M.W. Schmidt, K.K. Baldridge, J.A. Boatz, S.T. Elbert, M.S. Gordon, J.H. Jensen, S. Koseki, N. Matsunaga, K.A. Nguyen, S. Su, T.L. Windus, M. Dupuis, J.A. Montgomery, General atomic and molecular electronic structure system, J. Comput. Chaem., 14 (1993) 1347-1363.

[42] N. O'Boyle, A. Tenderholt, K. Langner, cclib: A library for package-independent computational chemistry algorithms, J. Comput. Chem. 29 (2008) 839-845

[43] G.H. Vineyard, Frequency factors and isotope effects in solid state rate processes, Journal of Physics and Chemistry of Solids, 3 (1957) 121-127.

[44] E. Vessally, S. Soleimani-Amiri, A. Hosseinian, L. Edjlali, A. Bekhradnia, A comparative computational study on the BN ring doped nanographenes, Applied Surface Science, 396 (2017) 740-745.

[45] P.A. Denis, F. Iribarne, Theoretical investigation on the interaction between beryllium, magnesium and calcium with benzene, coronene, cirumcoronene and graphene, Chemical Physics, 430 (2014) 1-6.

[46] S. Rasul, S. Suzuki, S. Yamaguchi, M. Miyayama, High capacity positive electrodes for secondary Mg-ion batteries, Electrochimica Acta, 82 (2012) 243-249.

[47] Y. Shao, M. Gu, X. Li, Z. Nie, P. Zuo, G. Li, T. Liu, J. Xiao, Y. Cheng, C. Wang, J.-G. Zhang, J. Liu, Highly Reversible Mg Insertion in Nanostructured Bi for Mg Ion Batteries, Nano Letters, 14 (2014) 255-260.

[48] X.-J. Ye, G.-L. Zhu, J. Liu, C.-S. Liu, X.-H. Yan, Monolayer, Bilayer, and Heterostructure Arsenene as Potential Anode Materials for Magnesium-Ion Batteries: A First-Principles Study, The Journal of Physical Chemistry C, 123 (2019) 15777-15786.

[49] J. Zhang, G. Liu, H. Hu, L. Wu, Q. Wang, X. Xin, S. Li, P. Lu, Graphene-like carbon-nitrogen materials as anode materials for Li-ion and mg-ion batteries, Applied Surface Science, 487 (2019) 1026-1032.

[50] N. Wu, Y.-C. Lyu, R.-J. Xiao, X. Yu, Y.-X. Yin, X.-Q. Yang, H. Li, L. Gu, Y.-G. Guo, A highly reversible, low-strain Mg-ion insertion anode material for rechargeable Mg-ion batteries, NPG Asia Materials, 6 (2014) e120-e120.

[51] Y.S. Meng, M.E. Arroyo-de Dompablo, First principles computational materials design for energy storage materials in lithium ion batteries, Energy & Environmental Science, 2 (2009) 589-609.